Large Deformation Numerical Modeling of Bucket Foundations Installation Using a Hypoplastic Model for Structured Clays

Chenyao Wei[1,*] and Teng Wang[2]

[1] College of Mechanical and Electronic Engineering, China University of Petroleum (East China), Qingdao 266580, China
[2] School of Petroleum Engineering, China University of Petroleum (East China), Qingdao 266580, China

*z23020010@s.upc.edu.cn

Abstract. Bucket foundations, favored for their low cost and ease of installation, have seen widespread adoption in marine renewable energy projects such as offshore wind farms. However, marine soils often exhibit high sensitivity, which can markedly influence soil strength and penetration resistance during installation. Traditional elastoplastic model models fall short in accurately capturing the nonlinear deformation and structural degradation of sensitive soils, leading to discrepancies in predicting foundation penetration performance. To address this challenge, this study adopts a hypoplastic constitutive model tailored for structured clays within the framework of critical state soil mechanics. The model introduces a structural parameter to describe the progressive breakdown of soil fabric and the associated reduction in strength under shear strain. A large-deformation numerical model was built in ABAQUS to reproduce the installation of bucket foundations in structured clay and to capture the associated soil-structure interaction. By integrating the RITSS method with the hypoplastic constitutive model that incorporates sensitivity evolution, comparative analyses were performed across varying initial sensitivities s_{ini} and degradation rates k. The results reveal how these parameters govern soil strength evolution and penetration behavior during installation.

Keywords: Large Deformation, Bucket Foundation, Hypoplastic Clay.

1 Introduction

The global transition toward low-carbon energy has fueled the rapid expansion of marine renewable energy, particularly offshore wind power. As the core load-bearing component of offshore structures, the foundation system fundamentally governs the project's overall stability, cost-effectiveness, and construction efficiency.

In practice, a bucket foundation is often constructed as a large-diameter steel caisson with a closed top and an open bottom. Typical geometries include a length of 3–30 m and a length-to-diameter ratio (L/D) in the range of 2–7. Its lightweight design, ease of

S. Sing et al. (eds.), *Proceedings of the 2025 7th International Conference on Civil Architecture and Urban Engineering (ICCAUE 2025)*, Atlantis Highlights in Engineering 43,
https://doi.org/10.2991/978-94-6239-682-1_10

installation, and reusability make it one of the most promising foundation solutions for offshore engineering. Installation begins with self-weight penetration, followed by suction-assisted penetration, where water and air are evacuated through valves at the top, creating a pressure differential between the bucket's interior and exterior. This suction drives the foundation to overcome soil resistance and embed itself to the desired depth. During this process, the skirt of the bucket disturbs the surrounding soil, leading to a progressive reduction in soil strength as shear strain accumulates, eventually resulting in a fully remolded state. Zhou [1] and Xiao [2] applied the Coupled Eulerian–Lagrangian (CEL) large-deformation finite element framework to study bucket foundation penetration in clay. By incorporating soil strain-softening, they analyzed not only the evolution of penetration resistance but also the accompanying soil flow patterns during installation. In a similar manner, Ma [3] used the CEL approach to account for both large deformation and softening effects, and further developed a penetration-resistance model for buckets with different external beveled tip angles. The results indicated that the external bevel angle plays a key role in governing soil softening intensity and, consequently, the soil plug height. Currently, there are still relatively few models for bucket foundation penetration that take into account large deformations and strain softening, with most existing studies relying on the low-precision CEL method and conventional constitutive models.

In the present study, the commercial software ABAQUS is employed to explore strain softening and strength degradation mechanisms during the installation of bucket foundations. A coupled large-deformation finite element method, incorporating a hypoplastic constitutive model for structured clay, is adopted to achieve a more accurate representation of soil behavior.

2 Numerical Model

2.1 Large Deformation Approach

In simulations of bucket foundation installation, the large penetration displacements involved often induce severe mesh distortion around the bucket skirt, leading to numerical instability and premature termination of the analysis. Consequently, conventional small-strain finite element formulations cannot reliably reproduce the entire penetration stage. To overcome this limitation, the Remeshing and Interpolation Technique with Small Strain (RITSS), developed within an effective-stress framework, provides a practical and well-validated solution to alleviate severe mesh distortion. Originally proposed by Hu and Randolph [4] for modeling large-deformation problems in geotechnical engineering—such as pile installation and extraction—RITSS decomposes a large deformation into a series of incremental small-deformation steps. In comparison to the CEL method, the RITSS approach delivers superior computational accuracy and facilitates a coupled analysis of effective stress and pore water pressure. The RITSS method has now been extensively adopted in the field of offshore geotechnical engineering [5-6].

As demonstrated by Wang [7], the Superconvergent Patch Recovery (SPR) technique is typically applied during the mapping stage. Leveraging the high-order accuracy

of sampling points, SPR reconstructs a smooth and high-fidelity effective stress field after each mesh update. The mapping procedure comprises three key steps: (1) recovering effective stress and constitutive parameters from sampling points to the nodes of the original mesh; (2) identifying, via spatial searching, the original element that contains each new Gauss point; and (3) performing polynomial interpolation to transfer the recovered nodal values to the new Gauss points. Because pore pressure is defined as a nodal variable, it requires no recovery step and can be directly mapped from old to new nodes.

2.2 Modeling Details

All numerical analyses in this study were carried out on the commercial finite element platform ABAQUS. An axisymmetric model was developed to simulate he penetration processes of the bucket foundation, as illustrated in Figure 1.

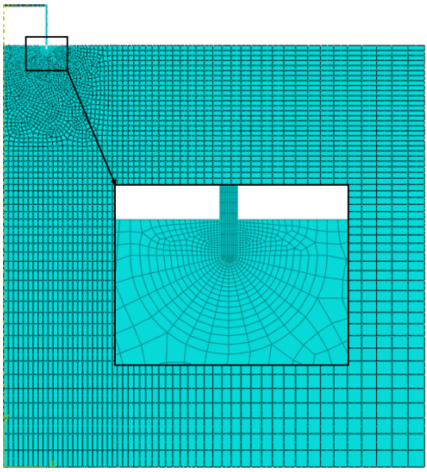

Fig. 1. Finite element model schematic.

The geometric and material parameters of the bucket foundation were adopted from Zhang [8]. In the numerical model, the foundation was treated as rigid, with a length-to-diameter ratio of 0.5 and a normalized wall thickness of 0.017D. Prior to penetration, the bucket was pre-embedded to a depth of 2t. To enhance numerical convergence, the lower edge of the bucket wall was rounded. The soil domain extended 5D in both vertical and horizontal directions to minimize boundary effects. To facilitate the use of the Superconvergent Patch Recovery (SPR) technique for recovering sampling point values to nodal points, the soil was discretized using second-order, eight-node, reduced-integration, axisymmetric pore-pressure elements (CAX8RP). A refined mesh zone was established by extending 4t outward from the bucket–soil interface, and 14 soil elements with a width of 0.002D were assigned along the contact zone adjacent to the bucket edge. The bucket–soil interaction was defined using a surface-to-surface contact algorithm. Hard contact was applied in the normal direction, while tangential behavior

was modeled using a penalty function with a friction coefficient μ = 0.2. The Soils analysis step was employed to account for fluid–solid coupling. Penetration was displacement-controlled, with a penetration increment of 0.005D per step.

2.3 Hypoplastic Constitutive Model for Structured Clay

The hypoplastic constitutive model [9] is capable of describing the inherently nonlinear response of geomaterials. Its governing relation can be expressed in the following general form:

$$\dot{\sigma} = f_s(L{:}\,\dot{\varepsilon} + f_d N \parallel \dot{\varepsilon} \parallel) \tag{1}$$

In this formulation, $\dot{\sigma}$ and $\dot{\varepsilon}$ denote Eulerian strain-rate tensor and the stress-rate tensor, respectively, while L and N are the fourth- and second-order constitutive tensors. Two scalar functions, f_s and f_d are employed to account for soil structure effects and densification-induced behavior, respectively. The hypoplastic model incorporates five constitutive parameters: the critical state friction angle φ_c, N, λ^*, κ^*, and v. The isotropic normal compression line (NCL) of the hypoplastic model is expressed as:

$$\ln(1+e) = N - \lambda^* \ln\left(\frac{p'}{p_r}\right) \tag{2}$$

For the preceding expression, the isotropic normal compression line is characterized by N and λ^*. In addition, e denotes the void ratio, p' denotes the mean effective stress, and the reference pressure is set to p_r = 1kPa. The parameter κ^* determines the slope of the isotropic unloading (reloading) line and, consequently, affects the compressibility of overconsolidated soils. φ_c denotes the critical-state friction angle, whereas v primarily controls the shear modulus of the material.

To model the softening and remolding behavior [10] of natural structured clays during the disturbance–reconsolidation process, the model defines sensitivity s as a deformation-dependent internal variable. Three additional parameters—k, A, and s_f—are introduced to describe its evolution. The evolution of sensitivity is governed by the following equation:

$$\dot{s} = -\frac{k}{\lambda^*}(s_{ini} - s_f)\sqrt{(\dot{\varepsilon}^v)^2 + \frac{A}{1-A}(\dot{\varepsilon}^s)^2} \tag{3}$$

In this formulation, k and A are parameters governing the rate of structural degradation, while s_{ini} and s_f denote the initial and ultimate sensitivities, respectively. $\dot{\varepsilon}^v$ and $\dot{\varepsilon}^s$ correspond to the plastic volumetric and plastic shear strain rates. The material parameters employed for the structured hypoplastic clay in this study are summarized in Table 1.

Table 1. Hypoplastic model parameters

Parameter	Value
φ_c	23°

λ^*	0.0811
κ^*	0.019
N	1.195
v	0.2
k	0.05,0.1,0.2
A	0.2
s_f	1
s_{ini}	1，2，5

3 Results and Discussions

3.1 Effect of Initial Sensitivity s_{ini}

The influence of initial sensitivity on soil degradation was analyzed first. Figure 2 compares the penetration responses of the bucket foundation for different initial sensitivities (s_{ini} = 1, 2, and 5) under a constant degradation rate (k = 0.05). The penetration resistance was normalized using q = V/A, where V is the penetration force and A is the vertical projected area of the bucket wall. The results show that the penetration resistance generally increases linearly with depth, but the growth rate is strongly governed by the initial sensitivity. Lower sensitivity yields higher resistance and a steeper slope, while higher sensitivity results in lower resistance and a gentler curve. The three curves exhibit minor differences in the early penetration stage (z/D = 0.1), but the discrepancies enlarge progressively with increasing depth, reaching a maximum at z/D = 0.5.

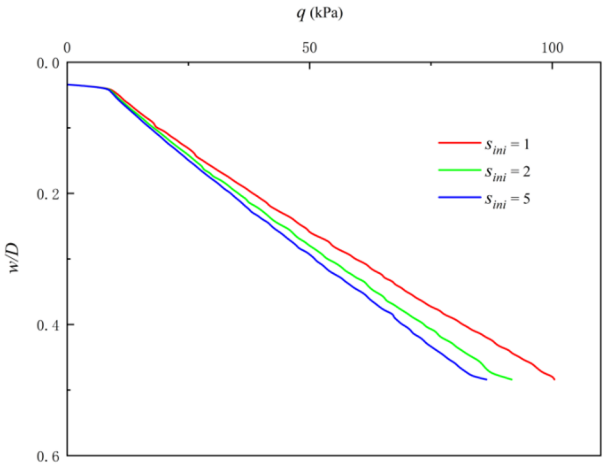

Fig. 2. Effect of sensitivity on penetration resistance.

The spatial evolution of undrained shear strength is further clarified, as illustrated in Figure 3. The soil away from the bucket wall exhibits an approximately linear strength

profile. Compared with the case without strength degradation (Figure 3a), the medium- and high-sensitivity conditions (Figures 3b and 3c) display denser strength contours, indicating steeper local gradients and more pronounced spatial variability.

A higher initial sensitivity reflects a more pronounced structural contrast between the intact and remolded soil, implying stronger initial structure. Under the same degradation rate, the shear strain induced by penetration accelerates structural breakdown, forming a thicker softened zone along the skirt and leading to greater strength reduction. Consequently, both side friction and tip resistance diminish, resulting in a lower total penetration resistance at the same depth.

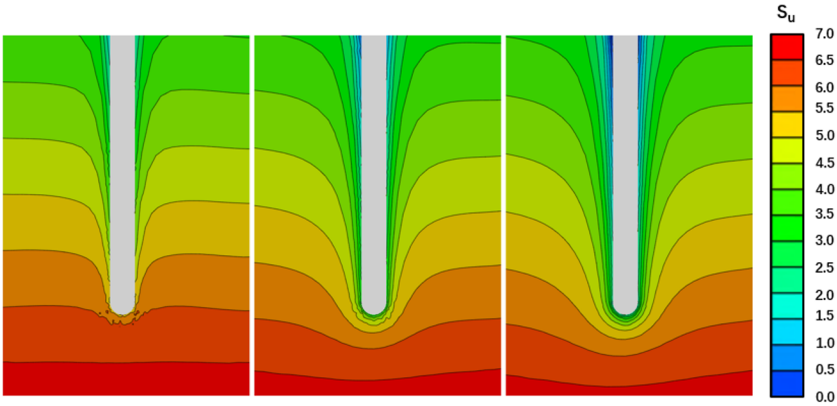

(a) $s_{ini} = 0.05$ (b) $s_{ini} = 0.1$ (c) $s_{ini} = 0.2$

Fig. 3. Undrained shear strength contours at different sensitivity.

3.2 Effect of Degradation Rate k

In addition to the effect of initial sensitivity, the sensitivity degradation rate k exerts a crucial influence on soil strength attenuation. Figure 4 illustrates the penetration responses of the bucket foundation under different degradation rates (k = 0.05, 0.1, and 0.2), with the initial sensitivity fixed at s_{ini} = 2. As penetration proceeds, higher degradation rates result in lower penetration resistance, and the divergence between the curves increases progressively with depth. The overall pattern closely resembles that of the cases with varying initial sensitivities under the same k, confirming that the degradation rate is likewise a critical factor controlling the strength degradation behavior of the soil. To further elucidate the mechanism by which the degradation rate k governs strength degradation, the state variable SDV14 (sensitivity s) was extracted at the end of penetration, and the corresponding sensitivity contours for three different k values are presented in Figure 5. All three cases demonstrate that a low-sensitivity zone develops along the bucket wall and progressively extends outward. With increasing k, the sensitivity contours become denser, and the low-s region thickens and expands, indicating that a larger portion of the soil mass experiences more intense structural breakdown and strength loss. This implies that shear-induced remolding accumulates more rapidly during penetration at higher k.

When k = 0.05 and 0.1, the minimum sensitivities are 1.263 and 1.097, respectively—indicating that no soil region has reached the fully remolded state ($s = s_{ini}$). In contrast, for k = 0.2, a circumferential band along the skirt tip reaches s = 1, signifying complete remolding in that area. The degradation rate k thus controls the rate at which sensitivity decays toward its final value. A higher k accelerates the transition from the undisturbed to the remolded condition under equivalent shear strain, enlarging the remolded soil volume. Consequently, both undrained shear strength and interface friction decrease more rapidly, leading to an overall reduction in penetration resistance.

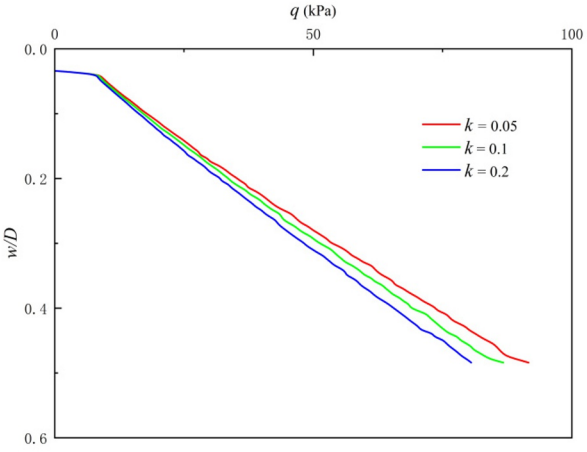

Fig. 4. Effect of degradation rate on penetration resistance.

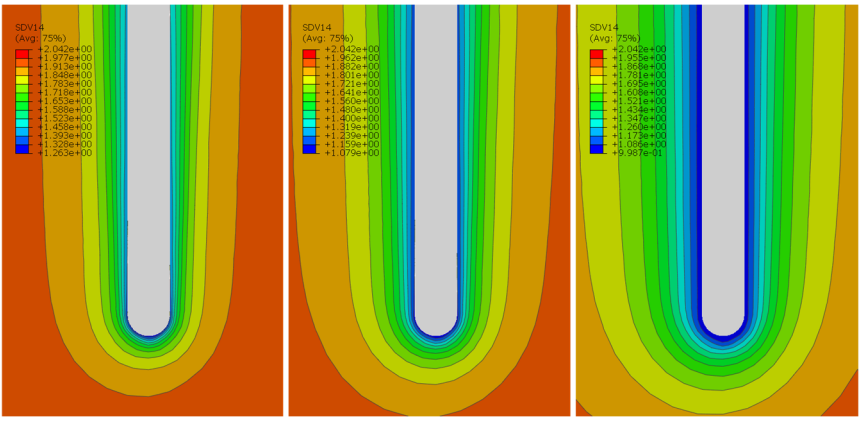

(a) $k = 0.05$ (b) $k = 0.1$ (c) $k = 0.2$

Fig. 5. Soil sensitivity contours at different degradation rates.

4 Conclusion and Outlook

In this study, a large-deformation finite element model was developed in ABAQUS, incorporating a structured hypoplastic clay constitutive framework to investigate the evolution of soil strength and bearing behavior of bucket foundations during installation.

Comparative analyses across different initial sensitivities s_{ini} and degradation rates k were performed to elucidate the soil softening mechanisms during penetration. The results demonstrate that s_{ini} reflects the degree of inherent soil structure: higher s_{ini} leads to a slower increase in penetration resistance with depth and more pronounced degradation of undrained shear strength. The parameter k dictates the rate of sensitivity decay: as k increases, the remolded zone surrounding the bucket skirt expands, and at k = 0.2, a portion of the soil reaches a fully remolded state, indicating that the shear strength has degraded to its ultimate value.

This study investigates the strength evolution and penetration resistance of bucket foundations in structured clay, while acknowledging several limitations. Firstly, it lacks a quantitative assessment of the influence of strain softening on skirt side friction, and does not detail the contribution of side friction to overall resistance or how this varies with sensitivity parameters. Secondly, the study overlooks the role of excess pore water pressure dissipation, accumulated during installation, in restoring soil strength. Accordingly, future research will incorporate the effects of side friction and conduct a consolidation analysis that integrates fluid-solid coupling.

References

1. Zhou, S., Zhou, M., Tian, Y., Zhang, X. Numerical investigation of caisson with pad-eye stiffener installation into nonhomogeneous clay. Applied Ocean Research, 121, 103077 (2022)
2. Xiao, Z., Zhang, D., Hu, P., Chang, Z., Yu, Z., Liu, X. Penetration resistance of tetrapod bucket foundations in clay considering soil large deformation and strength remoulding. Ocean Engineering, 329, 121113(2025)
3. Ma, T., Xiao, Z., Zhang, W., Hu, P., Wei, X. Effect of the external beveled tip angle of the bucket foundation in clay on its penetration resistance considering soil large deformation and strain softening. Ocean Engineering, 262, 112185(2022).
4. Hu, Y., Randolph, M. F. A practical numerical approach for large deformation problems in soil. International Journal for Numerical and Analytical Methods in Geomechanics, **22**(5), 327-350(1998)
5. Kou, H., Zhang, X., Huang, J. Fluid-solid coupling large deformation failure analysis of bucket foundations in saturated clay. Engineering Failure Analysis, 109807(2025)
6. Jerman, J., Mašín, D., Ragni, R., Bienen, B., Španiel, M. Aspects of soft clay behaviour important for correct prediction of spudcan foundation penetration. Computers and Geotechnics, 142, 104552(2022)
7. Wang, D., Hu, Y., Randolph, M. F. Effect of loading rate on the uplift capacity of plate anchors. In ISOPE International Ocean and Polar Engineering Conference, pp. ISOPE-I. ISOPE(2008)

8. Zhang, Y., Sun, L., Feng, X., Li, S. The consolidation response of skirted foundations in normally consolidated clay. Ocean Engineering, 296, 117064(2024)
9. Mašín, D. Clay hypoplasticity model including stiffness anisotropy. Géotechnique, **64**(3), 232-238(2014)
10. Cotecchia, F., Chandler, R. J. A general framework for the mechanical behaviour of clays. Géotechnique, **50**(4), 431-447(2000)